Structure *14*, 1099–1105, July 2006 ©2006 Elsevier Ltd All rights reserved DOI 10.1016/j.str.2006.05.015

How to Avoid Premature Decay of Your Macromolecular Crystal: A Quick Soak for Long Life

Ways & Means

Brice Kauffmann,[1] Manfred S. Weiss,[1] Victor S. Lamzin,[1] and Andrea Schmidt[1,*]

[1] EMBL Hamburg Outstation
c/o DESY
Notkestrasse 85
D-22603 Hamburg
Germany

Summary

Radiation damage to biological samples is currently one of the major limiting factors in macromolecular X-ray crystallography, since it severely and irreversibly affects the quality of the data that can be obtained from a diffraction experiment. However, radiation damage can effectively be reduced by utilizing the electron and radical scavenging potential of certain small-molecule compounds. We propose an approach to protect macromolecular crystals prior to data collection by quick soaking with scavengers. This, in favorable cases, can more than double crystal lifetime in the X-ray beam. The approach has the potential to yield diffraction data of superior quality and hence to increase the amount of high-quality diffraction data and of structural information attainable from a single crystal.

Introduction

Much of the currently available structural information on biological macromolecules has been obtained by bombarding the fragile macromolecule crystals with high-intensity X-rays in the energy range of typically 8–14 keV in order to produce X-ray diffraction patterns that can then be interpreted by using crystallographic methods. Inherent in such an experiment is the direct consequence of energy deposition in the sample, since, for typically used X-rays, the crystal absorbs about ten photons for each photon that is diffracted elastically. A cascade of ionization events and formation of radical species eventually damages the sample to an extent that limits the structural information that can be obtained from one crystal, both qualitatively and quantitatively. The advent of cryocrystallographic techniques in the early 1990s has alleviated this problem: crystals cooled to about 100 K exhibited a much longer lifetime in the beam than crystals at ambient temperature (see the review by Garman and Schneider [1997]). However, with the use of the highly intense wiggler and undulator beamlines at third-generation synchrotron radiation sources such as ESRF, APS, or SPring-8 from the late 1990s, radiation damage has again become a problem. Even more so, radiation damage is now often the limiting factor for the overall success of structure determination and is thought to be the underlying cause of most unsuccessful multiple anomalous dispersion (MAD) experiments (Murray and Garman, 2002), which require several data sets of high quality and isomorphism.

Radiation damage effects in crystals can be of general and/or specific nature. General damage manifests itself in the reduction of the overall scattering power of a crystal and can be monitored by following the increase in mosaicity, merging R factor, the Wilson B factor, and various other overall metrics (Murray and Garman, 2002). Specific radiation damage such as the breaking of disulfide bonds and the loss of carboxylate groups (Weik et al., 2000) is not as straightforward to detect. For that, other, more sensitive metrics need to be designed. As a quantitative monitor for radiation damage, Sliz et al. (2003) introduced the calculation of a merging R factor between the reflections occurring on the first image of a data set and those on subsequent images. Recently, Diederichs (2006) generalized the Sliz approach as the pairwise decay R factor (R_d) between identical and symmetry-related reflections as a function of image distance (the difference in frame number between the images on which the two compared reflections occur) (Diederichs, 2006). An increase of R_d as a function of image distance indicates structural changes occurring inside the crystal during data collection, making it a useful global indicator for radiation damage at the data processing stage.

While the effects of radiation damage on the protein structure can sometimes be successfully exploited for structure solution, as demonstrated by Ravelli and McSweeney (2000), or for the triggering of catalytic reactions (Berglund et al., 2002), in most cases it is essential to eliminate or correct for the effects of degradation in the diffraction data. Diederichs and coworkers proposed the "zero dose extrapolation" method (Diederichs et al., 2003), which is based on the observation that the intensity of single reflections changes as the data collection progresses (Blake and Phillips, 1962). Given a sufficient number of observations, the intensity of a reflection can be extrapolated to the time point of the data collection where no damage should have occurred. Over the last few years, a number of approaches have also been tried in order to reduce the radiation damage to the crystal and to extend crystal lifetime in the X-ray beam (Murray and Garman, 2002; O'Neill et al., 2002). These include the choice of wavelength of data collection (Müller et al., 2002) and cooling down the crystal to temperatures even lower than 100 K (Hanson et al., 2002). Furthermore, the introduction of potential electron and radical scavenging molecules has been mentioned in the literature (e.g., Blundell and Johnson, 1976), but very few compounds have been tested experimentally. The use of the small, aromatic molecule styrene as a scavenger was reported more than 30 years ago (Zaloga and Sarma, 1974; Sarma and Zaloga, 1975), and encouraging results have been recently achieved with ascorbic acid as a cocrystallizing agent by Murray and Garman (2002).

Here, we build up on the original ideas of Murray and Garman and present compounds that have the necessary chemical properties for acting as scavengers and

*Correspondence: andrea.schmidt@embl-hamburg.de

Table 1. Data Collection and Refinement Statistics for Lysozyme

	Native		Nicotinic Acid		Oxidized Glutathione		DTNB	
	set1	set5	set1	set5	set1	set5	set1	set5
Resolution limits (Å)	99.0–1.42 (1.47–1.42)	99.0–1.42 (1.47–1.42)	99.0–1.42 (1.47–1.42)	99.0–1.42 (1.47–1.42)	99.0–1.42 (1.47–1.42)	99.0–1.42 (1.47–1.42)	99.0–1.42 (1.47–1.42)	99.0–1.42 (1.47–1.42)
Unit cell parameters								
a (Å)	77.97	78.01	76.82	76.85	78.00	78.04	77.89	77.88
b (Å)	77.97	78.01	76.82	76.85	78.00	78.04	77.89	77.88
c (Å)	36.73	36.75	37.47	37.48	36.78	36.79	37.04	37.04
Mosaicity (°)	0.30	0.29	0.51	0.50	0.36	0.36	0.35	0.35
Total number of reflections	620,991	622,704	569,920	576,346	630,886	632,328	637,844	637,732
Redundancy	28.3	28.3	26.3	26.6	28.8	28.7	28.8	28.8
Completeness (%)	99.9 (99.4)	99.9 (99.8)	100 (100)	100 (100)	99.9 (100)	99.9 (100)	100 (100)	100 (100)
$I/\sigma(I)$	85.7 (17.9)	84.4 (15.7)	71.0 (8.1)	71.9 (7.2)	86.0 (18.0)	86.1 (15.7)	74.2 (7.5)	73.8 (6.8)
R_{merge} (%)	3.8 (20.3)	3.8 (23.7)	4.5 (24.0)	4.4 (24.6)	4.1 (22.9)	4.0 (25.4)	5.3 (43.6)	5.1 (48.7)
$R_{r.i.m.}$ (%)	3.9 (20.7)	3.9 (24.2)	4.6 (24.5)	4.5 (25.1)	4.1 (23.3)	4.1 (25.9)	5.3 (35.5)	5.2 (38.8)
$R_{p.i.m.}$ (%)	0.7 (4.0)	0.7 (4.7)	0.9 (4.7)	0.9 (4.8)	0.8 (4.4)	0.8 (4.9)	1.0 (9.0)	1.0 (10.1)
Optical resolution (Å)	1.20	1.23	1.31	1.31	1.22	1.23	1.29	1.30
Wilson B factor ($Å^2$)	13.9	14.6	19.4	19.9	14.4	15.2	17.1	17.7
R_{cryst} (%)	17.8	18.8	21.4	20.9	19.9	19.9	19.6	20.6
R_{free} (%)	20.3	20.2	25.3	24.5	22.0	22.0	21.9	22.6
Average B factor ($Å^2$)	14.9	15.3	18.5	19.5	16.3	16.2	17.0	16.8
Rmsd bond lengths (Å)	0.008	0.008	0.010	0.010	0.009	0.009	0.010	0.010
Rmsd bond angles (°)	1.3	1.2	1.3	1.3	1.2	1.2	1.2	1.3

For each crystal, the statistics are given for the first and the fifth sets of 360 images. Numbers in parentheses refer to the highest-resolution shell. $R_{r.i.m.}$: redundancy-independent merging R; $R_{p.i.m.}$: precision-indicating merging R. The optical resolution (as defined by *SFCHECK* [Vaguine et al., 1999; CCP4, 1994]) is the width of the origin peak of the Patterson synthesis and describes how close two electron density features can be in space to be resolvable.

that could be easily used both for cocrystallization and soaking, including quick-soaking (i.e., less than 30 s) experiments. The main aim is to reduce radiation damage to the macromolecular sample and to enhance both the success rate of structure determination and the quality of the resulting macromolecular models. From the vast number of potential substances, three different electron and radical scavenging molecules (nicotinic acid, 5,5′-dithio-bis-2-nitrobenzoic acid [DTNB], and oxidized glutathione) were chosen on the basis of their molecule size (less than 600 g/mol), chemical properties (presence of aromatic systems or disulphide bonds), and high solubility in aqueous solutions. These three compounds have been tested on three different protein systems. The method involves quick soaking of the crystals in the scavenger solution prior to their flash cooling for data collection. The scavenger quick-soaking approach has shown strong potential for yielding more structural information from a single protein crystal by slowing down its decay. We observed that, in most cases, the lifetime of the crystals in the X-ray beam could be prolonged and the diffraction data quality upheld over the time of data collection. Hence, structure determination (especially substructure solution from anomalous differences) may become easier and the refined models more accurate.

Results and Discussion

Quality of Diffraction Data and Refined Structures

The relevant data collection and refinement statistics of the data sets analyzed in this study are presented in Tables 1–3. All data sets are of high quality, and it is evident from the merging statistics that no significant harm has been done to the crystals by applying the quick-soaking method. In order to analyze the build-up of radiation damage, a number of successive data sets have been collected from each single crystal, and they were then compared. The experiments were purposely carried out on EMBL-Hamburg beamlines at the DORIS storage ring with moderate beam intensity in order to thoroughly monitor radiation damage induced slowly over time. The total dose to which the crystals were exposed was of the order of $4.5 * 10^6$ Gy, corresponding to about 20% of the "Henderson limit" (Henderson, 1990). The merging statistics between the first and last data sets of each series indicates that the extent to which the crystals were damaged by radiation is relatively small. The crystals from each protein were of comparable size, and for each of them, the full data set series was collected by using the same setup. This ensured that within one protein system the deposited dose in the crystals was always the same. The respective structures were refined against the first data set of a given series. There is no significant difference in refinement statistics for each structure of each series. The high accuracy of the refined structures allowed even weak features arising from radiation damage effects to be revealed in the difference electron density maps.

Quantitative Visualization of Radiation Damage in the Diffraction Data

The evolution of a pairwise R factor (R_d) as a function of the distance in frame number was used to monitor radiation damage. Figure 1A shows an example plot of the raw data and the corresponding linear fit for a native crystal in red and one soaked crystal in blue. Figures 1B–1D show the linear fit to the normalized R_d values for each of the 12 data set series. A straight line proved to be a good approximation to the observed dependences

Table 2. Data Collection and Refinement Statistics for Thaumatin

	Native		Nicotinic Acid		Oxidized Glutathione		DTNB	
	set1	set5	set1	set5	set1	set5	set1	set5
Resolution limits (Å)	99.0–1.50 (1.55–1.50)	99.0–1.50 (1.55–1.50)	99.0–1.50 (1.55–1.50)	99.0–1.50 (1.55–1.50)	99.0–1.50 (1.55–1.50)	99.0–1.50 (1.55–1.50)	99.0–1.50 (1.55–1.50)	99.0–1.50 (1.55–1.50)
Unit cell parameters								
a (Å)	57.41	57.51	57.97	57.99	57.62	57.67	58.03	58.07
b (Å)	57.41	57.51	57.97	57.99	57.62	57.67	58.03	58.07
c (Å)	149.97	150.14	150.15	150.22	150.03	150.15	150.30	150.40
Mosaicity (°)	0.31	0.48	0.65	0.63	0.41	0.48	0.76	0.75
Total number of reflections	579,933	561,800	561,670	559,615	525,396	505,321	561,511	561,180
Redundancy	14.2	13.7	13.7	13.6	12.9	12.5	13.7	13.7
Completeness (%)	99.9 (100)	99.9 (100)	99.8 (100)	99.8 (100)	99.6 (99.0)	98.7 (96.7)	99.9 (100)	99.9 (100)
$I/\sigma(I)$	57.1 (14.6)	53.8 (9.3)	49.2 (8.8)	44.0 (8.0)	45.5 (15.1)	42.9 (12.5)	38.5 (4.5)	38.2 (4.1)
R_{merge} (%)	4.8 (19.1)	4.7 (31.2)	5.0 (33.2)	5.2 (36.5)	5.6 (17.0)	6.3 (21.0)	6.3 (65.6)	6.6 (74.0)
$R_{r.i.m.}$ (%)	5.0 (19.8)	4.9 (32.4)	5.2 (34.5)	5.4 (37.9)	5.8 (17.7)	6.6 (21.9)	6.6 (68.2)	6.8 (76.8)
$R_{p.i.m.}$ (%)	1.3 (5.2)	1.3 (8.7)	1.4 (9.2)	1.5 (10.1)	1.6 (4.9)	1.8 (6.0)	1.8 (18.3)	1.9 (20.6)
Optical resolution (Å)	1.26	1.29	1.31	1.32	1.27	1.29	1.34	1.35
Wilson B factor ($Å^2$)	14.5	16.6	17.4	18.2	15.8	16.9	20.0	20.2
R_{cryst} (%)	17.0	18.7	20.2	20.2	18.9	18.9	19.9	19.8
R_{free} (%)	19.7	20.9	22.6	23.3	21.1	21.2	21.0	21.4
Average B factor ($Å^2$)	16.3	17.7	19.1	19.9	15.9	17.1	21.9	22.3
Rmsd bond lengths (Å)	0.005	0.009	0.008	0.009	0.008	0.008	0.008	0.009
Rmsd bond angles (°)	1.1	1.2	1.2	1.2	1.2	1.2	1.2	1.2

For each crystal, the statistics are given for the first and the fifth sets of 360 images. Numbers in parentheses refer to the highest-resolution shell. $R_{r.i.m.}$: redundancy-independent merging R; $R_{p.i.m.}$: precision-indicating merging R. The optical resolution (as defined by *SFCHECK* [Vaguine et al., 1999; CCP4, 1994]) is the width of the origin peak of the Patterson synthesis and describes how close two electron density features can be in space to be resolvable.

with a correlation coefficient ranging from 0.82 to 0.98. The slope of the straight line serves as a quantitative descriptor for the extent of radiation damage. Taking the native data set as a reference for each of the protein systems, significantly less damage occurs in the crystals soaked with scavengers prior to data collection.

Manifestation of Radiation Damage in the Protein Structures

Qualitatively, the radiation damage in the structures can be assessed by comparison of the highest positive and negative peaks in the difference electron density maps between the last and the first data set of a given series

Table 3. Data Collection and Refinement Statistics for Porcine Pancreatic Elastase

	Native		Nicotinic Acid		Oxidized Glutathione		DTNB	
	set1	set5	set1	set5	set1	set5	set1	set5
Resolution limits (Å)	99.0–1.55 (1.61–1.55)	99.0–1.55 (1.61–1.55)	99.0–1.55 (1.61–1.55)	99.0–1.55 (1.61–1.55)	99.0–1.58 (1.61–1.58)	99.0–1.58 (1.61–1.58)	99.0–1.65 (1.68–1.65)	99.0–1.65 (1.68–1.65)
Unit cell parameters								
a (Å)	50.48	50.50	50.04	50.06	50.40	50.42	50.67	50.68
b (Å)	58.02	58.03	57.61	57.62	58.01	58.02	58.07	58.07
c (Å)	74.49	74.49	74.40	74.42	74.51	74.53	74.90	74.90
Mosaicity (°)	0.62	0.69	0.48	0.48	0.84	0.83	0.32	0.32
Total number of reflections	467,676	468,435	462,745	457,332	414,830	4,433,491	385,999	386,119
Redundancy	14.4	14.4	14.5	14.3	14.5	14.3	14.5	14.5
Completeness (%)	99.7 (100)	99.5 (100)	99.9 (98.9)	99.9 (99.5)	100.0 (100)	100.0 (100)	99.9 (100)	99.5 (100)
$I/\sigma(I)$	47.4 (5.5)	47.3 (4.4)	74.9 (21.8)	72.5 (18.3)	58.9 (11.5)	39.8 (4.0)	50.3 (7.5)	49.5 (7.1)
R_{merge} (%)	6.2 (32.2)	6.1 (36.5)	3.6 (16.9)	3.9 (20.5)	4.8 (24.2)	7.7 (66.1)	6.2 (41.6)	6.1 (43.5)
$R_{r.i.m.}$ (%)	6.4 (29.2)	6.3 (34.3)	3.8 (17.6)	4.0 (21.2)	4.9 (25.1)	8.0 (68.6)	6.5 (43.1)	6.3 (45.1)
$R_{p.i.m.}$ (%)	1.7 (7.7)	1.7 (9.0)	1.0 (4.6)	1.1 (5.6)	1.3 (6.6)	2.1 (18.1)	1.7 (11.2)	1.7 (11.7)
Optical resolution (Å)	1.35	1.37	1.29	1.30	1.30	1.31	1.33	1.33
Wilson B factor ($Å^2$)	20.3	21.9	16.5	17.3	15.3	15.9	17.8	18.1
R_{cryst} (%)	16.9	17.9	18.0	18.1	18.1	18.2	18.2	18.2
R_{free} (%)	19.9	19.6	19.3	19.3	20.1	20.5	20.3	20.2
Average B factor ($Å^2$)	21.0	22.7	17.9	17.9	14.7	15.4	18.8	19.2
Rmsd bond lengths (Å)	0.008	0.009	0.010	0.010	0.008	0.009	0.010	0.010
Rmsd bond angles (°)	1.1	1.2	1.2	1.3	1.2	1.2	1.2	1.3

For each crystal, the statistics are given for the first and the fifth sets of 360 images. Numbers in parentheses refer to the highest-resolution shell. $R_{r.i.m.}$: redundancy-independent merging R; $R_{p.i.m.}$: precision-indicating merging R. The optical resolution (as defined by *SFCHECK* [Vaguine et al., 1999; CCP4, 1994]) is the width of the origin peak of the Patterson synthesis and describes how close two electron density features can be in space to be resolvable.

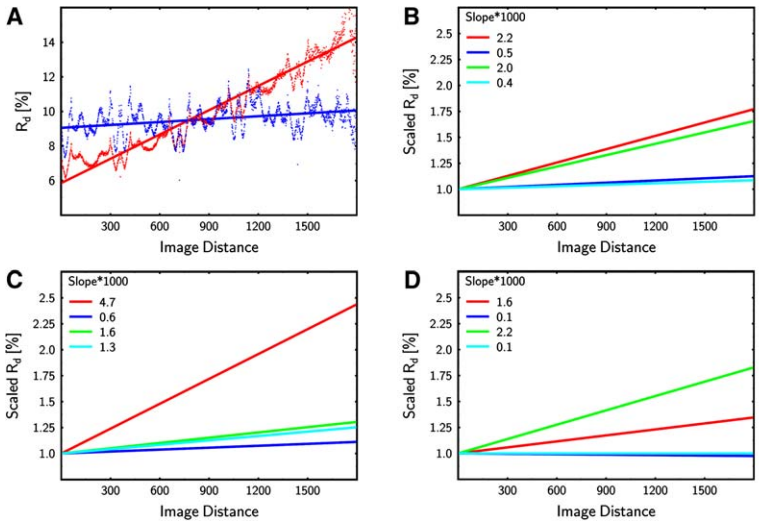

Figure 1. R_d Plots for the Data Sets from Each Protein System

(A) Raw R_d values (Diederichs, 2006) as a function of the distance in frame number for the thaumatin native (in red) and nicotinic acid-soaked (in blue) data. The linear fit to the data is also shown.

(B–D) Linearly approximated R_d^{norm} values for three crystal systems: (B) hen egg white lysozyme, (C) thaumatin, and (D) porcine pancreatic elastase. The red lines depict data of the native, unprotected crystal, while the blue, green, and cyan lines correspond to data collected from crystals soaked in 200 mM solutions of nicotinic acid, oxidized glutathione, and DTNB, respectively. The slopes of the linear fit, given in each plot, are multiplied by a factor of 1000 to make the comparison easier, and they indicate the extent of radiation damage to the data: the larger the slope, the larger the damage. The total rotation range covered is 1800° for lysozyme and porcine pancreatic elastase and 900° for thaumatin.

(Figure 2). Soaking with scavenging molecules prior to data collection generally led to a reduction of strong features in such a difference map. In all cases, this agreed with the decrease of the slopes in the R_d plots. The specific observations made on the three proteins and the effects of each of the tested scavengers are presented in the following sections.

Hen Egg-White Lysozyme

The comparison of the plots (Figure 1B) shows a similar level of damage in the native data and in the data collected on the glutathione-soaked crystal. However, in this particular experiment, nicotinic acid and DTNB show considerable potential as scavengers. According to the R_d values, the level of radiation damage reached after five data sets of 360° in the presence of nicotinic acid or DTNB corresponded to the damage level after only one data set of 360° for the native and glutathione-soaked crystals, thus indicating an up to five times longer lifetime for those crystals.

The analysis of the positive and negative difference peaks in the ($F_{o,end} - F_{o,start}$, $\alpha_{calc,start}$) maps (Figures 2A–2D) was in agreement with the slopes calculated from the R_d plots. HEWL contains four disulfide bridges, with Cys76-Cys94 being the one most sensitive to radiation (Weik et al., 2000; Murray and Garman, 2002). In the native, i.e., unprotected, data, all four disulfide groups were damaged, and the ablation of the carboxylic groups of Asp52, Glu7, and the amide and amine groups of Gln41 and Lys13 was observed. Whereas the damage to the disulphide bridges Cys6-Cys127, Cys30-Cys115, and Cys64-Cys80 could be reduced to some extent by the scavengers, Cys76-Cys94 appeared to be damaged already after the first data set of 360°, even in the presence of scavengers (data not shown). Comparing the protection by nicotinic acid and DTNB, we observed that all disulfide bridges, but none of the other sites, were damaged in the structure with DNTB, whereas the disulfide bridge Cys64-Cys80 was protected in the structure with nicotinic acid, but the carboxylic group of Asp52 was not. Apparently these two compounds, while effectively reducing the overall radiation damage effects in a similar manner, function by entirely different mechanisms and show a selective mode of protection of chemical groups in the protein. No tightly bound scavenger molecule was found in the refined structures.

Thaumatin

In this particular case, almost the same positive effect of all scavengers on the reduction of radiation damage was observed (Figure 1C). The native data are severely affected, as reflected by the high slope value from the R_d plot. By examining the maps (Figures 2E–2H), it became clear that the reduction of the damage is substantial with all scavengers. The DTNB map is the one showing the least differences, confirming the high protective potential of this molecule. In addition to the eight disulfide bridges, many other sites are affected as well and show damage in all structures. However, only the native unprotected structure has all of the following sites damaged: Asp70, Lys67, Asp147, Thr160, Arg125, Glu168, and Glu156. Moreover, in this native structure, a tartrate molecule from the crystallization buffer was also damaged, and two peaks in the difference maps were observed on carbonyl groups of the main chains of Cys71 and Cys159, indicating the beginning of the breakdown of the main chain and hence the most severe observed damage in our three model systems.

Porcine Pancreatic Elastase

As observed for HEWL, glutathione is not able to protect porcine pancreatic elastase (PPE) crystals (Figures 2I–2L). On the contrary, the data collected in the presence of glutathione were even more affected by the radiation effects than the native data. In the corresponding structures, the sites affected most by the damage were all four disulfide bridges as well as Asp154, Glu6, Asp178, Asp87, Glu185, Thr33, and Met41 (Figure 2I).

In our experiment, the most sensitive site in the PPE structure is the disulfide bridge Cys30-Cys46, although Weiss et al. (2005) had reported that in the structure of the PPE/Cd^{2+} complex the disulfide bridge Cys158-Cys174 was the most susceptible one. According to

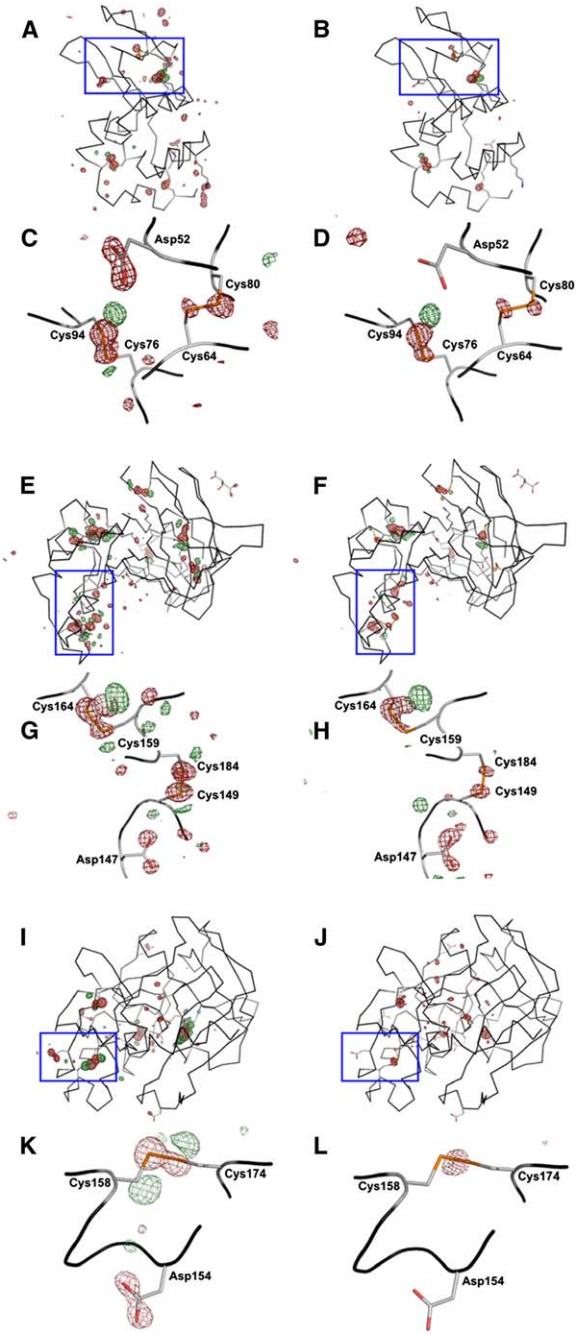

Figure 2. Electron Density Maps Computed with the Coefficients $F_{o,end} - F_{o,start}$ and $\alpha_{c,start}$

(A–L) The qualifier "start" indicates the first data set of 360 images, and the qualifier "end" indicates the fifth data set of 360 images of each series. Disappearing electron density is represented in red, and appearing density in shown in green. (A)–(D) depict the maps for HEWL, (E)–(H) for thaumatin, and (I)–(L) for PPE. In each of the panels, the unprotected case (left two panels) is compared with the most efficiently protected case (right two panels). (A) and (B) present the difference maps superimposed with the overall lysozyme native and DTNB-soaked structures, respectively. (C) and (D) show two close-up views of the same structures to highlight the specific effects observed. The close-up regions are indicated by blue rectangles. For easier visualization, different orientations for the close-up regions were chosen. The same representations are shown in (E)–(H) and (I)–(L) for the thaumatin and PPE crystals, respectively; both the thaumatin and PPE crystals are protected with nicotinic acid. The maps are contoured at the same +5σ and −5σ levels to ensure comparability.

the difference maps in the DTNB structure, only the disulphide bridges and Met41, but none of the other residues, were damaged, whereas in the nicotinic acid structure, the disulphide bridges and two of the carboxylic groups (Asp154 and Asp178) were destroyed. This concurs with the observation made for HEWL discussed above. Also, no tightly bound scavenger molecule was found in the structure.

Conclusions

A significant reduction of radiation damage in the presence of particular scavenging molecules was observed in all three protein systems under investigation. Except for the lysozyme case, glutathione is the least effective, whereas both nicotinic acid and DTNB protect the protein crystals well. The degree of protection was different for the different scavengers and the different chemical groups in the proteins. This suggests different protection mechanisms depending on a number of factors, including the chemical properties of the scavenger molecules and their activity to the various radical species formed upon irradiation. Additional experiments will be required on more protein systems, as well as the exploration of more soaking conditions, in order to investigate these specific effects in more depth.

The scavenger quick-soaking method provides an easy-to-apply approach to combat radiation damage in macromolecular crystals for a number of proteins. Consequently, higher quality X-ray data, higher redundancy, and possibly higher resolution data may be obtained from a single crystal. Since for a given scavenger compound similar effects are observed in three different proteins, it may be expected that comparable protection would be achieved for other proteins. Our results strongly indicate the need to consider the addition of scavengers, most notably DTNB and nicotinic acid into the preparation of the crystals for X-ray data collection, in parallel to the search for suitable cryoconditions.

Experimental Procedures

Crystallization

The proteins used for crystallization were commercially available and used without further purification. Crystallization experiments were carried out at 293 K by using the vapor-diffusion hanging-drop technique. Crystals of hen egg-white lysozyme (HEWL) (Calbiochem product no. 4403, lot no. B43266) were grown as described by Weiss et al. (2000) by mixing equal amounts of protein solution (30 mg/ml in water) and reservoir solution containing 50 mM sodium acetate (pH 4.5) and 5% (w/v) sodium chloride. The tetragonal crystals (space group $P4_32_12$) appeared within a few days and exhibited unit cell parameters of a = 78.7 and c = 37.2 Å. Porcine pancreatic elastase (PPE) (Serva product no. 20929, lot no. 16461) was crystallized in the presence of calcium ions as described by Weiss et al., (2002). A protein solution of 12 mg/ml was mixed with an equal volume of reservoir solution composed of 0.1 M sodium acetate (pH 5.1), 0.2 M sodium citrate, and 0.04 M calcium chloride. Crystals belonging to space group $P2_12_12_1$ with unit cell parameters of a = 49.3, b = 57.0, and c = 73.3 Å appeared within a few days. Thaumatin (Sigma product no. T-7638, lot no. 108F0299) was crystallized by mixing equal amounts of protein solution (15 mg/ml in 0.1 M N-(2-acetamido)iminodiacetic acid [ADA] [pH 6.5]) and reservoir solution (0.1 M ADA [pH 6.5], 1 M sodium/potassium tartrate) by

following the recipe of Charron et al., (2002). The tetragonal crystals (space group $P4_12_12$) grew within a few days. They exhibit cell parameters of a = 57.3 and c = 148.8 Å and diffract to beyond 1.5 Å resolution.

Crystal Preparation

Nicotinic acid (Sigma product no. N4126), oxidized glutathione (Sigma product no. G9027), and 5,5′-dithio-bis-2-nitrobenzoic acid (DTNB, Sigma product no. D8130) were used as purchased without further purification. Solutions (200 mM) of each compound were freshly prepared by dissolving the powder in the reservoir solution directly in the wells of the crystallization plate. Prior to data collection, a crystal was then fished from the crystallization drop and immersed quickly (less than 20 s) in the respective scavenger solution. All crystals were then cryoprotected by using dry paraffin oil in order to ensure that the solvent remained unaltered and to ensure that no additional molecules, e.g., glycerol, were introduced into the system.

Diffraction Data Collection

Diffraction data sets were collected at three different X-ray diffraction beamlines (X11, X13, and BW7A operating at wavelengths of 0.81 Å) at EMBL Hamburg, DESY on a single-axis goniostat with a 165 mm MAR CCD detector. The relevant data collection details are given in Tables 1–3. Exposure times were chosen in order to utilize the full dynamic range of the detector without allowing too many overloaded reflections. Varying incident beam intensity was compensated for by carrying out the data collection in dose mode, with the speed of rotation of the spindle axis dependent on the incident beam intensity. For each crystal, 360 images were collected 5 consecutive times. This corresponds to 5 × 360° in the HEWL and PPE cases (1° oscillation width) and 5 × 180° for thaumatin, for which data were collected with a 0.5° oscillation width due to the presence of one long cell axis. The total exposure time (dose) for thaumatin was the same as for the other proteins. The starting spindle angle for the first data set was chosen arbitrarily. All data set series (native and three soaked crystals) for each of the proteins were collected from crystals with approximately the same size and from the same crystallization drop. In order to be able to compare the different data sets within one series to each other to the largest extent possible, all data sets from a given protein were collected on the same beamline, by using the same wavelength, the same detector, and the same exposure time. In order to ensure high data redundancy and high quality of the resulting maps needed for monitoring the structural changes, a set of 360 images was used as one data set for each protein. A cutoff of 1.4–1.6 Å to the maximum diffraction limit was chosen as a compromise between straightforward, fast data collection and high enough resolution for monitoring structural changes.

Data Processing

Data were indexed and integrated with DENZO and were scaled in SCALEPACK (Otwinowski and Minor, 1997). The postrefinement procedure in SCALEPACK was used to refine the cell parameters and the mosaicity for each data set. The redundancy-independent merging R factor, $R_{r.i.m.}$, as well as the precision-indicating merging R factor, $R_{p.i.m.}$ (Weiss, 2001), were calculated by using the program RMERGE.

Analysis of Decay

As an indicator for radiation damage, an R_d plot (Diederichs, 2006) has been computed for each data set series. R_d is defined as a pairwise R factor between identical and symmetry-related reflections occurring on different diffraction images. A positive slope in the plot indicates significant radiation damage, and the value of the slope indicated the extent of damage. For a convenient visual comparison, the various plots were shifted to a common y axis intercept of 1.0 by using a normalized R_d (R_d^{norm}) as defined below.

$$R_d^{norm}(n) = 1 + \frac{R_d(n) - R_d(1)}{R_d^{native}(1)}, \quad (1)$$

where n is the difference in frame numbers and R_d (1) is the pairwise R factor for reflections observed on consecutive images within the data set.

Refinement

Structures have been refined to the highest resolution possible against the first data set of each series by using the program REFMAC5 (Murshudov et al., 1997). Relevant refinement statistics are given in Tables 1–3.

Difference Fourier Maps

To investigate the radiation damage at a structural level, difference electron density maps were calculated with the amplitudes $F_{o,end} - F_{o,start}$ and the phases $\alpha_{c,start}$; the identifier "start" stands for the first data set in each series, and the identifier "end" stands for the last one. The phases $\alpha_{c,start}$ are taken from the model refined against the first data set in each series. A positive peak in such an electron density map indicates structural features that are gained upon radiation damage, whereas a negative peak indicates structural features that are lost upon radiation damage.

Acknowledgments

The authors thank Dr. Elspeth Garman (University of Oxford, UK) for comments and discussion. This work was supported by the European Commission 6th Framework Programme "Life Sciences, Genomics and Biotechnology for Health" (Integrated Research project BIOXHIT, Contract No. LHSG-CT-2003-503420).

Received: December 12, 2005
Revised: May 3, 2006
Accepted: May 3, 2006
Published: July 18, 2006

References

Berglund, G.I., Carlsson, G.H., Smith, A.T., Szoke, H., Henriksen, A., and Hajdu, J. (2002). The catalytic pathway of horseradish peroxidase at high resolution. Nature *417*, 463–468.

Blake, C.C.F., and Phillips, D.C. (1962). Effects of X-irradiation on single crystals of myoglobin. In Biological Effects of Ionizing Radiation at the Molecular Level (Vienna: International Atomic Energy Agency), pp. 183–191.

Blundell, T.L., and Johnson, L.N. (1976). Protein Crystallography (New York: Academic Press).

CCP4 (Collaborative Computational Project, Number 4) (1994). The CCP4 suite: programs for protein crystallography. Acta Crystallogr. D. Biol. Crystallogr. *50*, 760–763.

Charron, C., Kadri, A., Robert, M.-C., Giegé, R., and Lorber, B. (2002). Crystallization in the presence of glycerol displaces water molecules in the structure of thaumatin. Acta Crystallogr. D Biol. Crystallogr. *58*, 2060–2065.

Diederichs, K. (2006). Some aspects of quantitative analysis and correction of radiation damage. Acta Crystallogr. D Biol. Crystallogr. *62*, 96–101.

Diederichs, K., McSweeney, S., and Ravelli, R.B. (2003). Zero-dose extrapolation as part of macromolecular synchrotron data reduction. Acta Crystallogr. D Biol. Crystallogr. *59*, 903–909.

Garman, E., and Schneider, T.R. (1997). Macromolecular cryocrystallography. J. Appl. Crystallogr. *30*, 211–237.

Hanson, B.L., Harp, J.M., Kirschbaum, K., Schall, C.A., DeWitt, K., Howard, A., Pinkerton, A.A., and Bunick, G.J. (2002). Experiments testing the abatement of radiation damage in D-xylose isomerase crystals with cryogenic helium. J. Synchrotron Radiat. *9*, 375–381.

Henderson, R. (1990). Cryo-protection of protein crystals against radiation damage in electron and X-ray diffraction. Proc. R. Soc. Lond. Biol. Sci. *241*, 6–8.

Müller, R., Weckert, E., Zellner, J., and Drakopoulous, M. (2002). Investigation of radiation-dose-induced changes in organic light-atom crystals by accurate d-spacing measurements. J. Synchrotron Radiat. *9*, 368–374.

Murray, J., and Garman, E. (2002). Investigation of possible free-radical scavengers and metrics for radiation damage in protein cryo-crystallography. J. Synchrotron Radiat. *9*, 347–354.

Murshudov, G.N., Vagin, A.A., and Dodson, E.J. (1997). Refinement of macromolecular structures by the maximum-likelihood method. Acta Crystallogr. D Biol. Crystallogr. *53*, 240–255.

O'Neill, P., Stevens, D.L., and Garman, E.F. (2002). Physical and chemical considerations of damage induced in protein crystals by synchrotron radiation: a radiation chemical perspective. J. Synchrotron Radiat. *9*, 329–332.

Otwinowski, Z., and Minor, W. (1997). Processing of X-ray diffraction data collected in oscillation mode. Methods Enzymol. *276*, 307–326.

Ravelli, R.B., and McSweeney, S.M. (2000). The 'fingerprint' that X-rays can leave on structures. Structure *8*, 315–328.

Sarma, R., and Zaloga, G. (1975). Structure studies on styrene-treated immunoglobulin crystals. J. Mol. Biol. *98*, 479–484.

Sliz, P., Harrison, S.C., and Rosenbaum, G. (2003). How does radiation damage in protein crystals depend on X-ray dose? Structure *11*, 13–19.

Vaguine, A.A., Richelle, J., and Wodak, S.J. (1999). SFCHECK: a unified set of procedures for evaluating the quality of macromolecular structure-factor data and their agreement with the atomic model. Acta Crystallogr. D Biol. Crystallogr. *55*, 191–205.

Weik, M., Ravelli, R.B., Kryger, G., McSweeney, S., Raves, M.L., Harel, M., Gros, P., Silman, I., Kroon, J., and Sussman, J.L. (2000). Specific chemical and structural damage to proteins produced by synchrotron radiation. Proc. Natl. Acad. Sci. USA *97*, 623–628.

Weiss, M.S. (2001). Global indicators of X-ray data quality. J. Appl. Crystallogr. *34*, 130–135.

Weiss, M.S., Palm, G.J., and Hilgenfeld, R. (2000). Crystallization, structure solution and refinement of hen egg-white lysozyme at pH 8.0 in the presence of MPD. Acta Crystallogr. D Biol. Crystallogr. *56*, 952–958.

Weiss, M.S., Panjikar, S., Nowak, E., and Tucker, P.A. (2002). Metal binding to porcine pancreatic elastase: calcium or not calcium. Acta Crystallogr. D Biol. Crystallogr. *58*, 1407–1412.

Weiss, M.S., Panjikar, S., Mueller-Dieckmann, C., and Tucker, P.A. (2005). On the influence of the incident photon energy on the radiation damage in crystalline biological samples. J. Synchrotron Radiat. *12*, 304–309.

Zaloga, G., and Sarma, R. (1974). New method for extending the diffraction pattern from protein crystals and preventing their radiation damage. Nature *251*, 551–552.